Sound velocity softening in body-centered cubic niobium under shock compression

Xiaohong Li (李孝红) [1,*] Chao Yang (杨超) [2,*] Bo Gan (甘波) [1] Yuqian Huang (黄钰倩) [1] Qiming Wang (王齐明) [1]
Toshimori Sekine (関根利守) [3] Jiawang Hong (洪家旺) [4] Gang Jiang (蒋刚) [1,5,†] and Youjun Zhang (张友君) [1,5,‡]

[1] *Institute of Atomic and Molecular Physics, Sichuan University, Chengdu 610065, China*
[2] *Department of Physics, Jishou University, Hunan 416000, China*
[3] *Center for High Pressure Science and Technology Advanced Research, Shanghai 201203, China*
[4] *School of Aerospace Engineering, Beijing Institute of Technology, Beijing 100081, China*
[5] *Key Laboratory of High Energy Density Physics and Technology of Ministry of Education, Sichuan University, Chengdu 610065, China*

Our understanding of pressure-induced anomalies in the physical and mechanical properties of Nb with a simple body-centered cubic structure remains limited both experimentally and theoretically. In this work we experimentally investigate the sound velocity of the compressional, bulk, and shear waves of Nb up to about 69 GPa and 1100 K under shock compression. These measurements reveal a significant softening in both the compressional and shear wave sound velocities in Nb compressed at 50 to 60 GPa. First-principles computations indicate that this anomalous behavior is most likely due to a pressure-induced Lifshitz-type electronic topological transition at 50 to 60 GPa. This study thus indicates that high-order phase transformations associated with the changes of electronic structures play an important role in the physical modification of transition metals.

I. INTRODUCTION

Transition metals form various crystal structures because the structural energy depends on the filling of the d bands in the periodic table [1]. Under high pressure and temperature (P-T) conditions, a number of transition metals experience a series of first- or higher-order phase transformations [2,3]. Understanding the phase transformations and the underlying mechanisms of transition metals at high P-T is of significant importance in materials science, condensed-matter physics, and planetary science [4,5]. The phase stability and physical properties of group-VB transition metals (V, Nb, and Ta) at high P-T have been extensively studied both theoretically and experimentally [6–9]. They have one of the simplest crystal structures (body-centered cubic, bcc) [10], but have complex physical properties at extreme conditions [11], such as electronic topological transitions [12], Fermi-surface nesting [13], nonadiabatic correction [14,15], and strong electron-phonon coupling [16,17].

Niobium (Nb) is a typical $4d$ transition metal of group-VB, with the highest superconducting transition temperature ($T_c = 9.25$ K) among transition metals under ambient pressure [18–20]. It is also one of the most promising refractory metals due to its high melting point and good ductility at room temperature [21–25]. Early static and dynamic high-pressure studies show that Nb retains its bcc phase at pressures up to 174 GPa [26,27]. Conversely, theoretical studies predicted softening anomalies of the elastic constants of Nb under high pressure [11–14,18]. For example, first-principles total energy

calculations predict an elastic constant softening of Nb at about 50 GPa [13], which is explained by the nesting vector $\boldsymbol{q}_n$ going to zero at the Fermi surface. Koči *et al.* [18] investigated the Fermi surface of Nb via first-principles calculations and reported that the Fermi surface has a shrinking nesting vector at about 74 GPa, which may result in an abnormal softening of the shear elastic constant C_{44}. In addition, theoretical calculations based on density functional theory (DFT) found that a striking softening of elastic constants C_{44} and $C' = (C_{11}-C_{12})/2$ in Nb occurs at about 60 GPa [14], which may be caused by the underlying rhombohedral distortion. Although these theoretical studies indicate a pressure-induced elastic modulus anomaly at 50 to 70 GPa, the mechanisms behind this anomaly remain controversial, and experimental evidence is also absent. Therefore, further investigations by both theoretical calculations and high P-T experiments [28] are urgently needed to understand the elastic modulus anomaly of Nb under extreme conditions.

This paper presents an investigation into the sound velocity of bcc Nb at high P-T under shock compression using a two-stage light gas gun. The compressional (V_P), bulk (V_b), and shear (V_S) sound-wave velocities of Nb were measured up to about 69 GPa and 1100 K. The results reveal softening anomalies for both V_P and V_S in Nb at 50 to 60 GPa. The three-dimensional (3D) Fermi surfaces of Nb calculated using DFT shows that a pressure-induced Lifshitz-type electronic topological transition (ETT) in Nb provides the main contribution to the elastic modulus softening.

II. METHODS OF EXPERIMENT AND COMPUTATION

High-purity (>99.95%) polycrystalline bcc Nb was used as the starting material. Its initial density was measured by

---

*These authors contributed equally to this work.

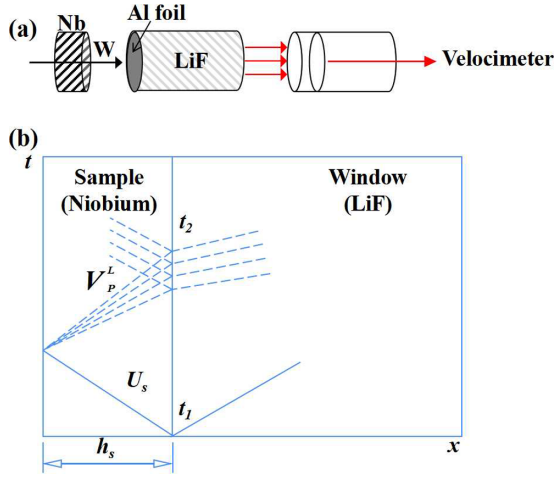†gjiang@scu.edu.cn

‡zhangyoujun@scu.edu.cn

FIG. 1. (a) Schematic diagram of experimental configuration for sound velocity measurements and (b) Lagrangian x-t diagram for reverse-impact experiments. h_s is the sample thickness, U_S is the propagation velocity of the shockwave in the sample, V_P^L is the Lagrangian velocity of the release wave in the sample, and t_1 and t_2 are the arrival times of the shockwave and unloading wave at the sample-LiF window interface, respectively.

using the Archimedean principle to be 8.597 to 8.620 g/cm^3. The sample was machined into 1.5-mm-thick disks with a diameter of 24 mm. Shock experiments were carried out using a 25-mm-bore two-stage light gas gun at the Institute of Atomic and Molecular Physics, Sichuan University, China. Reverse-impact configurations were used to measure the sound velocity of Nb at high P-T, as shown in Fig. 1(a). Single-crystal lithium fluoride (LiF) of [100] orientation (15-mm diameter and 5-mm thickness) was used as the window [29]. Aluminum foil ($\approx$10 μm) was coated onto the front surface of the LiF window. The velocity of the flyer was measured by using a magnetic-induced diagnostic system with an uncertainty of roughly 0.5%. The particle velocity

profile at the impact interface was measured by using an all-fiber displacement interferometer system for any reflector [30]. The sound velocities of Nb were then determined by applying the optical analyzer technique with uniaxial strain loading (in the direction of shockwave propagation) [28,31]. Figure 1(b) shows the principle for wave interactions between Nb and LiF during the impact process. Nine reverse-impact experiments were done in a P-T range of 27 to 69 GPa and 400 to 1100 K. Table I details the impact conditions and experimental results. The measured particle velocity profiles at the Nb-LiF interface indicate a plastic single-wave structure at the investigated shock pressures, as shown in Fig. 2.

The ABINIT code [32] was used for structural optimization and electronic structure calculations with the Troullier-Martins norm-conserving pseudopotentials and local density approximation (LDA) [33]. The kinetic-energy cutoff was determined to be 35 hartree, and the Monkhorst-Pack scheme with a 30 × 30 × 30 Γ-centered k-point mesh was used. The total energy was converged to within 1×10^{-8} hartree. The Gaussian smearing method was used to describe the electronic occupations with a broadening set to 0.015. The 3D Fermi surface was visualized using the FermiSurfer code [34]. The computation details can be found elsewhere [12]. The Vienna *ab initio* simulation package, VASP [35,36], was used to calculate the enthalpy of Nb under high pressure. The atomic electronic structures were described by the projector augmented wave approximation with the LDA [36,37]. The kinetic-energy cutoff was set to 350 eV, and the Γ-centered k-point mesh was set to 30 × 30 × 30. An energy convergence criterion of 10^{-6} eV and a maximum Hellmann-Feynman force on each atom of less than 10^{-3} eV/Å were used to ensure the accuracy of the interatomic forces.

III. RESULTS AND DISCUSSION

The particle velocity U_P and shockwave velocity U_S in shock-compressed Nb can be calculated by using the impedance-matching method based on the measured impact

TABLE I. The experimental conditions and results of Nb by reverse-impact experiments. ρ_0 is the initial density of Nb at ambient conditions measured using the Archimedean method. W is the impact velocity. U_P and U_S are the particle velocity and shockwave velocity of the compressed sample, respectively, where $U_S = C_0 + \lambda U_P$. P is the Hugoniot pressure. T_H is the shock temperature of Nb [39]. The known Hugoniot of LiF and Nb are from Ref. [38] (LiF: $\rho_0 = 2.638$ g/cm^3, $C_0 = 5.148$ km/s, $\lambda = 1.358$; Nb: $\rho_0 = 8.587$ g/cm^3, $C_0 = 4.46$ km/s, $\lambda = 1.20$). V_P^L and V_b^L are the measured Lagrangian sound velocities of the compressional and bulk waves, respectively. V_P, V_b, and V_S are the Eulerian sound velocities of the compressional, bulk, and shear waves, respectively. A detailed analysis of the uncertainties in sound velocities is given in the Supplemental Material [42].

| Shot No.	ρ_0 (g/cm^3)	W (km/s)	U_P (km/s)	U_S (km/s)	P (GPa)	V_P^L (km/s)	V_P (km/s)	V_b^L (km/s)	V_b (km/s)	V_S (km/s)	Est. T_H (K)
1	8.597 ± 0.009	2.07 ± 0.01	0.596 ± 0.012	5.426 ± 0.074	27.8 ± 0.7	6.793 ± 0.149	6.047 ± 0.134	6.037 ± 0.102	5.374 ± 0.092	2.402 ± 0.298	439 ± 50
2	8.604 ± 0.003	2.53 ± 0.01	0.787 ± 0.011	5.103 ± 0.041	34.6 ± 0.6	7.597 ± 0.153	6.425 ± 0.131	6.480 ± 0.105	5.481 ± 0.090	2.902 ± 0.251	493 ± 70
3	8.609 ± 0.002	3.17 ± 0.01	0.996 ± 0.012	5.404 ± 0.030	46.3 ± 0.6	8.432 ± 0.169	6.878 ± 0.139	7.459 ± 0.109	6.084 ± 0.090	2.779 ± 0.297	651 ± 55
4	8.607 ± 0.001	3.30 ± 0.01	1.030 ± 0.013	5.559 ± 0.031	49.3 ± 0.7	8.851 ± 0.182	7.211 ± 0.149	7.700 ± 0.112	6.273 ± 0.093	3.080 ± 0.298	686 ± 50
5	8.606 ± 0.001	3.54 ± 0.01	1.123 ± 0.015	5.562 ± 0.031	53.8 ± 0.8	8.537 ± 0.161	6.813 ± 0.130	–	–	–	762 ± 75
6	8.602 ± 0.005	3.72 ± 0.01	1.170 ± 0.011	5.756 ± 0.021	57.9 ± 0.6	8.811 ± 0.163	7.020 ± 0.131	7.959 ± 0.107	6.341 ± 0.086	2.608 ± 0.307	840 ± 60
7	8.596 ± 0.009	3.75 ± 0.02	1.186 ± 0.012	5.713 ± 0.023	58.2 ± 0.6	8.747 ± 0.163	6.931 ± 0.131	7.884 ± 0.106	6.247 ± 0.086	2.600 ± 0.304	846 ± 60
8	8.604 ± 0.007	4.05 ± 0.02	1.310 ± 0.010	5.684 ± 0.016	64.1 ± 0.5	10.076 ± 0.211	7.754 ± 0.163	8.423 ± 0.124	6.482 ± 0.097	3.685 ± 0.287	957 ± 70
9	8.609 ± 0.002	4.26 ± 0.02	1.370 ± 0.013	5.864 ± 0.019	69.2 ± 0.7	10.787 ± 0.230	8.037 ± 0.178	8.676 ± 0.134	6.649 ± 0.104	3.910 ± 0.304	1075 ± 80
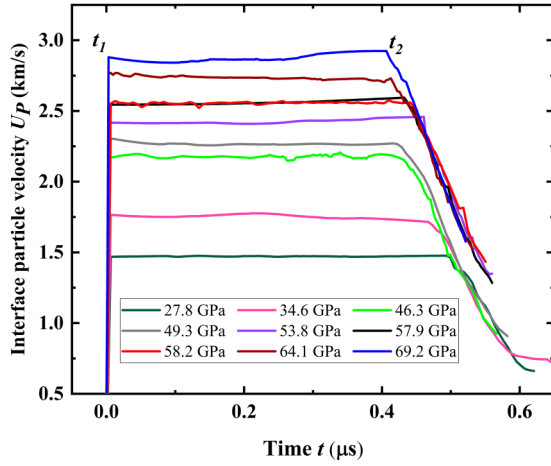
FIG. 2. Particle velocity profiles at the Nb-LiF interface measured by using the all-fiber displacement interferometer system for any reflector under shock compression. The impact velocity and corresponding pressure-temperature conditions are listed in Table I. t_1 and t_2 are the arrival times of the shockwave and release wave at the interface, respectively.

velocity W of the flyer and the particle velocity at the Nb-LiF interface. The results for U_S and U_P are listed in Table I. The density ρ in the Hugoniot state of Nb is then determined by

$$\rho = \frac{\rho_0}{\left(1 - \frac{U_P}{U_S}\right)},\tag{1}$$

where ρ_0 is the initial density of Nb at ambient conditions. The pressure-density (P-ρ) Hugoniot data in this study are entirely consistent with the previous shock compression experiments [27], as shown in Fig. 3(a). The Hugoniot temperature of Nb [Fig. 3(b)] is estimated by using the theoretical calculation from Ref. [39].

The shockwave was generated by impact at time t_1. When it propagated to the rear interface of the sample, a release wave was emitted forward through the sample at the compressional sound velocity at high pressure. The arrival of the release wave at the sample-window interface reduces the particle velocity at time t_2 [Fig. 1(b)]. Thus, the Lagrangian compressional sound velocity V_P^L can be determined based on the travel time $\Delta t = t_2 - t_1$ by using [40,41]

$$V_P^L = \frac{h_s}{\Delta t - \frac{h_s}{U_s}},\tag{2}$$

where h_s is the thickness of the Nb sample and U_S is the shockwave velocity of the compressed sample. The uncertainty of the result for Δt is typically less than 1% (see Fig. S1 in the Supplemental Material [42]). The Eulerian compressional sound velocity V_P can be converted from V_P^L based on

$$V_P = \frac{\rho_0}{\rho} V_P^L.\tag{3}$$

The bulk sound velocity V_b of Nb cannot be directly obtained by the particle velocity profiles due to the Bauschinger effect [43]. Thus, Asay *et al.* [44] proposed a method to determine V_b at the Hugoniot state by linearly extrapolating the plastic unloading part to the Hugoniot state in the relationship of V_P and U_P. By using this method, we obtain V_b for Nb along
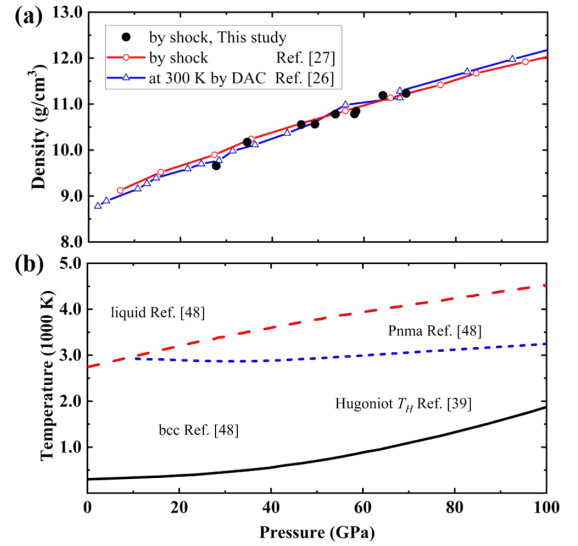

FIG. 3. Hugoniot equation of state and pressure-temperature relation in Nb under shock compression. (a) The P-ρ Hugoniot relationship of Nb under shock compression. The black filled circles represent the measured density in this work. The open circles and triangles are the literature data of the density under shock [27] and under static compression by a diamond-anvil cell [26], respectively. (b) Hugoniot temperature T_H calculated by canonical *ab initio* molecular dynamics with the parameterization of Perdew, Burke, and Ernzerhof simulations [39]. The blue dashed line indicates the bcc-Pnma phase boundary of Nb determined by high-P-T x-ray diffraction experiments and *ab initio* quantum molecular dynamics simulations [48]. The red dashed line is the melting curve of Nb at high pressure fitted to the Simon-Glatzel formula by Errandonea *et al.* [48].

the Hugoniot and a typical plastic unloading portion of the velocity history (e.g., shot No. 4 at about 49.3 GPa in Fig. 4). Based on the results for V_P and V_b, the shear sound velocity V_S
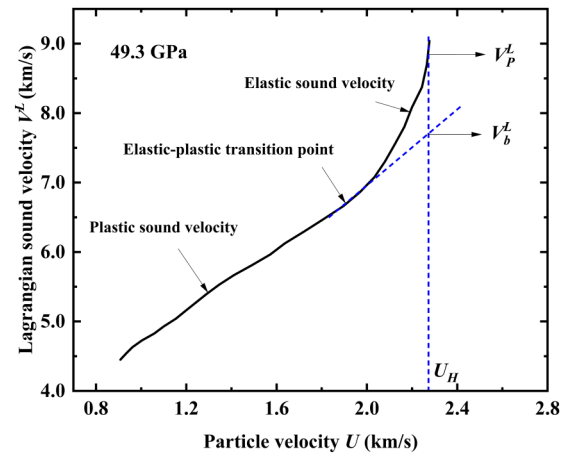

FIG. 4. Typical results for Lagrangian sound velocity of Nb as a function of particle velocity at a shock pressure of about 49.3 GPa. V_P^L is the Lagrangian compressional sound velocity. U_H is the particle velocity of Nb in the Hugoniot state. V_b^L is the Lagrangian bulk sound velocity that can be plastically extrapolated from the relationship between V_P^L and U_P in the unloading portion.
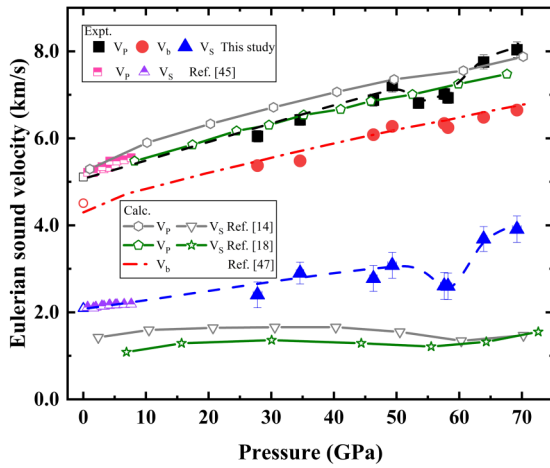
FIG. 5. Eulerian compressional (V_P), bulk (V_b), and shear (V_S) sound velocities of Nb as a function of shock pressure. The open symbols (black square, red circle, and blue triangle) show V_P (5.11 km/s), V_b (4.5 km/s), and V_S (2.09 km/s) of Nb at ambient conditions, respectively [46]. The filled symbols (black squares, red circles, and blue triangles) are the measured V_P, V_b, and V_S of Nb, respectively, under shock compression. The red dash-dotted line is the theoretically predicted bulk sound velocity at high pressure and room temperature [47]. The pink semi-squares and purple semi-triangles are the measured sound velocity of polycrystalline Nb at room temperature using ultrasonic measurements in conjunction with synchrotron x-ray diffraction [45]. The open gray hexagons and inverted triangles [14], and open green pentagons and pentagrams [18] are the sound velocities at high pressure and 0 K derived from the elastic constants by first-principles computations and density functional theory, respectively.

can be determined by using [43]

$$V_S^2 = \frac{3}{4}\left(V_P^2 - V_b^2\right). \tag{4}$$

The experimental results show that the V_P and V_S of Nb continuously increase from about 6.05 to 7.21 km/s, and from about 2.40 to 3.08 km/s with increasing shock pressure from ∼27.8 to 49.3 GPa (Fig. 5), respectively. An extrapolation of these results to low pressures is consistent with previous measurements made with a multi-anvil apparatus using ultrasonic measurements and synchrotron x-ray diffraction at 300 K [45] and below 10 GPa. However, the sound velocity above 50 GPa indicates a significant softening of both V_P and V_S at the pressures of 50 to 60 GPa (Fig. 5). Conversely, the measured V_b monotonically increases with increasing pressure without abnormality up to about 70 GPa, which is overall consistent with previous predictions derived from the isothermal bulk modulus at 298 K (Fig. 5) [47].

Figure 5 compares several theoretical results for the sound velocity of Nb at high pressures. For example, both Koči *et. al.* [18] and Wang *et al.* [14] used DFT to predict the softening of the shear wave sound velocity V_S (or shear elastic constant C_{44}) of Nb above about 50 GPa (Fig. 5). The proposed anomaly may result primarily from a nesting vector that shrinks with pressure [18] or an underlying rhombohedral distortion [14]. However, the softening of compressional velocity V_P (or elastic constant C_{11}) for Nb is not well explained at similar pressures.
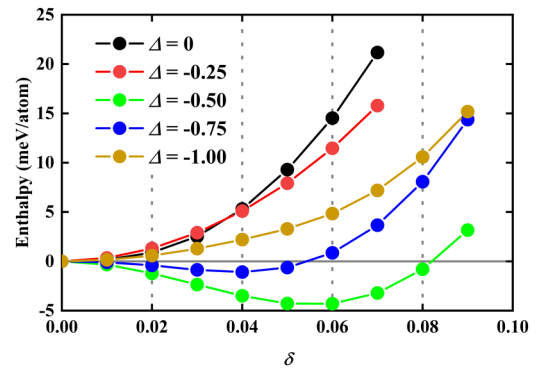

FIG. 6. Calculated enthalpy of Nb as a function of the rhombohedral deformation parameter (δ) between bcc and the distorted bcc phase at 57 GPa. Δ is the charge transfer in Nb. The bcc phase is the most stable phase, with $\Delta = 0$. When the Fermi level is reduced by removing electrons ($\Delta < 0$), the rhombohedral phase becomes more stable than the bcc phase.

As seen in Fig. 3(b), Nb remains in the bcc structure in the *P-T* range investigated in this study. Thus, the softening of the sound velocities V_P and V_S in compressed Nb should not be caused by a solid-solid phase transition. To understand the elastic modulus anomaly in compressed Nb near 60 GPa, we first consider the possible rhombohedral distortion (or the competition between bcc and rhombohedral structure). Under high pressure, the domain wall or extrinsic anisotropic strain may lead to charge transfer [49,50], so we calculated the enthalpy difference between pristine bcc Nb and distorted bcc Nb as a function of the rhombohedral deformation parameter δ at 57 GPa (see results in Fig. 6). The charge transfer Δ is set to zero for bcc Nb at 57 GPa. The Fermi level shifts upon removing electrons (i.e., $\Delta = -0.25$), so the rhombohedral structure becomes more stable. This rhombohedral phase may become the most stable structure in Nb when $\Delta = -0.5$ at 57 GPa. However, removing more electrons may destabilize the rhombohedral structure and lead back to the bcc phase when $\Delta < -1$. The charge-transfer-induced bcc-rhombohedral phase transition may contribute to the elastic modulus and thus lead to an abnormal softening in compressed Nb near 57 GPa [14,51]. The distorted bcc Nb may occur when it alloys with fewer *d*-electron elements (e.g., its left neighbor, zirconium [11]). In addition, both V_P and V_S undergo an abnormal softening in this experiment. However, the underlying rhombohedral mechanism explains only the abnormity of the shear modulus [14]. In the present experiments, pristine bcc Nb with high purity was used to retain the bcc phase structure in the investigated *P-T* range based on the known *P-T* phase diagram [48]. Therefore, we consider other suitable mechanisms to explain both the V_P and V_S abnormalities for Nb at 50 to 60 GPa.

To better understand the sound-velocity softening in Nb at 50 to 60 GPa, we calculated its 3D Fermi surfaces at high pressure by using the DFT code ABINIT [32]. The total energy of bcc Nb with different energy cutoffs and k-point meshes was simulated to obtain the proper parameters based on the total energy difference below 1 mHa/atom [52] (see Fig. S2 in the Supplemental Material [42]). The theoretical results show that the geometry of the 3D Fermi surface broadens
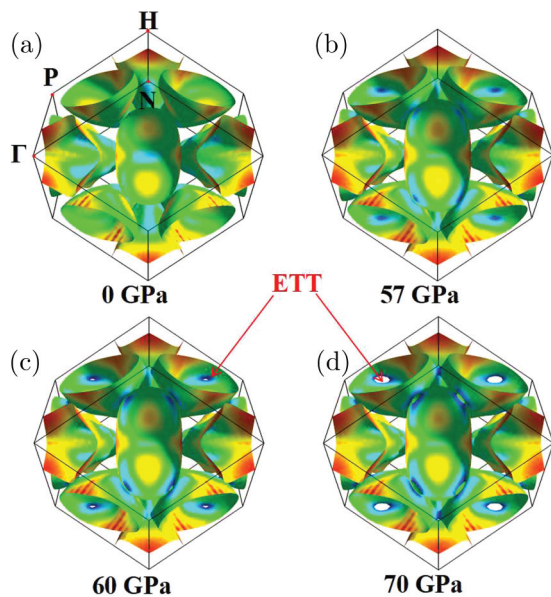
FIG. 7. 3D Fermi surfaces in bcc Nb calculated by using DFT. Fermi surfaces of Nb at (a) ambient pressure, (b) 57 GPa, (c) 60 GPa, and (d) 70 GPa. A Lifshitz-type ETT occurs at about 60 GPa in Nb, where the new voids appear at the Fermi surfaces and grow with increasing pressure (e.g., to about 70 GPa).

upon increasing pressure to 57 GPa at 0 K, but does not undergo any topological change with respect to the topology at ambient pressure [Figs. 7(a) and 7(b)]. Upon further increasing the pressure, a pressured-induced Lifshitz-type ETT occurs near 60 GPa [Fig. 7(c)], where new voids form in the Fermi surfaces. These voids grow upon increasing the pressure to 70 GPa [Fig. 7(d)]. To confirm the Lifshitz-type ETT in compressed bcc Nb, we also calculate the 3D Fermi surfaces with different values of tsmear (e.g., tsmear = 0.15, 0.01, and 0.005), which describes the state occupation by electrons near the Fermi surface at various finite temperatures. The calculations indicate that the ETT in bcc Nb occurs under compression, even when changing the value of tsmear. Given that the 3D Fermi surface describes the structure of the electron-occupied states near the Fermi level, decreasing tsmear from 0.15 to 0.01 to 0.005 changes only slightly the 3D Fermi surface, corresponding to the transition pressures from roughly 60 GPa down to 52 and 47 GPa, respectively (see Fig. S3 in the Supplemental Material [42]). As a result, the calculated Fermi surfaces indicate that the ETT of Nb should occur at 50 to 60 GPa, which is consistent with the significant softening in V_P and V_S at 50 to 60 GPa. We therefore suggest that the ETT most likely causes the observed elastic modulus softening under shock compression.

When using the simplest model of oscillations of ions placed in the electron sea, the compressional sound velocity V_P of metals may be expressed as [53]

$$V_P{}^2 = (n/M)/[1/\nu(\mu)], \qquad (5)$$

where n is the density of conduction electrons, M is the mass of the unit cell, and $\nu(\mu)$ is the electron density of states (DOS) per unit volume. Under high pressure, the ETT may cause a singularity in the DOS [12], which may lead to an

anomaly in the compressional sound velocity V_P. The bulk sound velocity V_b of Nb increases smoothly with increasing pressure; so, according to Eq. (4), V_S could undergo a softening similar to that of V_P. Therefore, the sound-velocity softening for Nb observed at 50 to 60 GPa is most likely caused by the ETT near the Fermi surface.

The pressure-induced ETT occurs in group-VB transition metals and may significantly affect their physical and mechanical properties. For instance, the elastic softening of C_{44} and C' is predicted to occur at about 200 GPa for vanadium [13,54] because of the transition in the electronic system. The anomalies in elastic constants (C_{11} and C_{44}) and in the mechanical properties (shear modulus, Young's modulus, and bulk modulus) of tantalum also occur at about 100 GPa and are caused by an ETT [12]. Pressure-induced ETT is also ubiquitous in many other transition metals [55]. For example, the ETT can change the Debye sound velocity of hcp iron at about 40 GPa [56]. Lattice parameters, compressibility, and elastic constants can be modified in 4d metals such as cadmium [57,58] due to ETTs under high-pressure conditions. Lifshitz-type ETTs have also been predicted in the 5d metal osmium at high pressure [59], which may cause the anomalies of its lattice parameters c/a ratio. These results indicate that the pressure-induced ETT, commonly existing as a 2.5-order phase transition, can significantly modify the physical properties of condensed matter.

IV. CONCLUSION

We herein study the density and sound velocities of polycrystalline bcc Nb at high P-T up to about 69 GPa and 1100 K under shock compression. The pressure-density Hugoniot data of Nb produce a smooth curve with no solid-phase transition under the investigated P-T conditions. A strong softening in V_P and V_S of Nb occurs at 50 to 60 GPa, and normal behavior is recovered upon further increasing the pressure. The 3D Fermi surfaces calculated by using DFT indicate that the softening is most likely induced by a Lifshitz-type ETT. Overall, pressure-induced ETT is ubiquitous and plays an important role in physical modifications in transition metals. This work is significant for better understanding the physical and mechanical properties of materials under extreme conditions.

[1] H. L. Skriver, Phys. Rev. B **31**, 1909 (1985).

[2] L. V. Al'tshuler and A. A. Bakanova, Sov. Phys. Usp. **11**, 678 (1969).

[3] I. M. Lifshitz, Zh. Eksp. Teor. Fiz. **38**, 1569 (1960); Sov. Phys. JETP **11**, 1130 (1960).

[4] C. Pépin, G. Geneste, A. Dewaele, M. Mezouar, and P. Loubeyre, Science **357**, 382 (2017).

[5] B. Martorell, L. Vočadlo, J. Brodholt, and I. G. Wood, Science **342**, 466 (2013).

[6] A. Landa, P. Söderlind, I. I. Naumov, J. E. Klepeis, and L. Vitos, Computation **6**, 29 (2018).

[7] Y. S. Yao and D. D. Klug, Phys. Rev. B **88**, 054102 (2013).

[8] L. Burakovsky, S. P. Chen, D. L. Preston, A. B. Belonoshko, A. Rosengren, A. S. Mikhaylushkin, S. I. Simak, and J. A. Moriarty, Phys. Rev. Lett. **104**, 255702 (2010).

[9] D. Antonangeli, D. L. Farber, A. Bosak, C. M. Aracne, D. G. Ruddle, and M. Krisch, Sci. Rep. **6**, 31887 (2016).

[10] Y. Nakagawa and A. D. B. Woods, Phys. Rev. Lett. **11**, 271 (1963).

[11] A. Landa, P. Söderlind, A. V. Ruban, O. E. Peil, and L. Vitos, Phys. Rev. Lett. **103**, 235501 (2009).

[12] Y. J. Zhang, C. Yang, A. Alatas, A. H. Said, N. P. Salke, J. W. Hong, and J-F. Lin, Phys. Rev. B **100**, 075145 (2019).

[13] A. Landa, J. Klepeis, P. Söderlind, I. Naumov, O. Velikokhatnyi, L. Vitos, and A. Ruban, J. Phys.: Condens. Matter **18**, 5079 (2006) .

[14] Y. X. Wang, H. Y. Geng, Q. Wu, X. R. Chen, and Y. Sun, J. Appl. Phys. **122**, 235903 (2017).

[15] N. A. Lanzillo, J. B. Thomas, B. Watson, M. Washington, and S. K. Nayak, Proc. Natl. Acad. Sci. USA **111**, 8712 (2014).

[16] D. Lamago, M. Hoesch, M. Krisch, R. Heid, K. P. Bohnen, P. Böni, and D. Reznik, Phys. Rev. B **82**, 195121 (2010).

[17] C. M. Varma, E. I. Blount, P. Vashishta, and W. Weber, Phys. Rev. B **19**, 6130 (1979).

[18] L. Koči, Y. Ma, A. R. Oganov, P. Souvatzis, and R. Ahuja, Phys. Rev. B **77**, 214101 (2008).

[19] J. Trivisonno, S. Vatanayon, M. Wilt, J. Washick, and R. Reifenberger, J. Low Temp. Phys. **12**, 153 (1973).

[20] V. V. Struzhkin, Y. A. Timofeev, R. J. Hemley, and H. K. Mao, Phys. Rev. Lett. **79**, 4262 (1997).

[21] Y. T. Zou, X. T. Qi, X. B. Wang, T. Chen, X. F. Li, D. Welch, and B. S. Li, J. Appl. Phys. **116**, 013516 (2014).

[22] J. S. Tse, Z. Q. Li, K. Uehara, Y. M. Ma, and R. Ahuja, Phys. Rev. B **69**, 132101 (2004).

[23] C. M. Varma and W. Weber, Phys. Rev. B **19**, 6142 (1979).

[24] J. R. Slining and D. A. Koss, Metall. Mater. Trans. B **4**, 1261 (1973).

[25] C. T. Sims, High Temp. Technol. **2**, 185 (1984).

[26] T. Kenichi and A. K. Singh, Phys. Rev. B **73**, 224119 (2006).

[27] R. G. McQueen, S. P. Marsh, J. W. Taylor, J. N. Fritz, and W. J. Carter, in *High Velocity Impact Phenomena*, edited by R. Kinslow (Academic Press, New York, 1970), p. 293.

[28] Y. Y. Yu, Y. Tan, C. D. Dai, X. M. Li, Y. H. Li, Q. Wu, and H. Tan, Appl. Phys. Lett. **105**, 201910 (2014).

[29] P. A. Rigg, M. D. Knudson, R. J. Scharff, and R. S. Hixson, J. Appl. Phys. **116**, 033515 (2014).

[30] J. D. Weng, H. Tan, X. Wang, Y. Ma, S. L. Hu, and X. S. Wang, Appl. Phys. Lett. **89**, 111101 (2006).

[31] T. S. Duffy and T. J. Ahrens, J. Appl. Phys. **82**, 4259 (1997).

[32] X. Gonze *et al.*, Comput. Phys. Commun. **248**, 107042 (2020).

[33] N. Troullier and J. L. Martins, Phys. Rev. B **43**, 1993 (1991).

[34] M. Kawamura, Comp. Phys. Commun. **239**, 197 (2019).

[35] G. Kresse and J. Hafner, Phys. Rev. B **47**, 558 (1993).

[36] G. Kresse and J. Furthmüller, Phys. Rev. B **54**, 11169 (1996).

[37] G. Kresse and J. Furthmüller, Comput. Mater. Sci. **6**, 15 (1996).

[38] *LASL Shock-Wave Hugoniot Data*, edited by S. P. Marsh (Univ. California Press, Berkeley, 1980).

[39] P. F. Weck, J. P. Townsend, K. R. Cochrane, S. D. Crockett, and N. W. Moore, J. Appl. Phys. **125**, 245905 (2019).

[40] J. B. Hu, C. D. Dai, Y. Y. Yu, Z. J. Liu, Y. Tan, X. M. Zhou, H. Tan, L. C. Cai, and Q. Wu, J. Appl. Phys. **111**, 033511 (2012).

[41] J. B. Hu, X. M. Zhou, H. Tan, J. B. Li, and C. D. Dai, Appl. Phys. Lett. **92**, 111905 (2008).

[42] See Supplemental Material at http://link.aps.org/supplemental/10.1103/PhysRevB.105.104110 for the uncertainty analysis of the measured sound velocities, the calculation details for Nb with different energy cutoffs and k-point meshes, and Fermi surfaces of Nb with different tsmear parameters under high pressures.

[43] J. B. Hu, X. M. Zhou, C. D. Dai, H. Tan, and J. B. Li, J. Appl. Phys. **104**, 083520 (2008).

[44] J. R. Asay and L. C. Chhabildas, in *Shock Waves and High-Strain-Rate Phenomena in Metals*, edited by M. A. Mayers and L. E. Murr (Plenum, New York, 1981), p. 417.

[45] Y. T. Zou, Y. Li, H. Y. Chen, D. Welch, Y. S. Zhao, and B. S. Li, Appl. Phys. Lett. **112**, 011901 (2018).

[46] E. B. Zaretsky and G. I. Kanel, J. Appl. Phys. **120**, 105901 (2016).

[47] P. I. Dorogokupets, T. S. Sokolova, B. S. Danilov, and K. D. Litasov, Geodyn. Tectonophysics **3**, 0067 (2012).

[48] D. Errandonea, L. Burakovsky, D. L. Preston, S. G. MacLeod, D. Santamaría-Perez, S. Chen, H. Cynn, S. I. Simak, M. I. McMahon, J. E. Proctor, and M. Mezouar, Commun. Mater. **1**, 60 (2020).

[49] L. Romaner, G. Heimel, J. L. Brédas, A. Gerlach, F. Schreiber, R. L. Johnson, J. Zegenhagen, S. Duhm, N. Koch, and E. Zojer, Phys. Rev. Lett. **99**, 256801 (2007).

[50] S. Bedwani, D. Wegner, M. F. Crommie, and A. Rochefort, Phys. Rev. Lett. **101**, 216105 (2008).

[51] Y. X. Wang, Q. Wu, X. R. Chen, and H. Y. Geng, Sci. Rep. **6**, 32419 (2016).

[52] A. H. Romero *et al.*, J. Chem. Phys. **152**, 124102 (2020).

[53] Y. M. Blanter, M. L. Kaganoy, A. V. Panisulaya, and A. A. Varlamo, Phys. Rep. **245**, 0370 (1994).

[54] A. Landa, J. Klepeis, P. Söderlind, I. Naumov, O. Velikokhatnyi, L. Vitos, and A. Ruban, J. Phys. Chem. Solids **67**, 2056 (2006).

[55] Y. Akahama, M. Kobayashi, and H. Kawamura, J. Phys. Soc. Jpn. **60**, 3211 (1991).

[56] K. Glazyrin, L. V. Pourovskii, L. Dubrovinsky, O. Narygina, C. McCammon, B. Hewener, V. Schünemann, J. Wolny, K. Muffler, A. I. Chumakov, W. Crichton, M. Hanfland, V. B. Prakapenka, F. Tasnadi, M. Ekholm, M. Aichhorn, V. Vildosola, A. V. Ruban, M. I. Katsnelson, and I. A. Abrikosov, Phys. Rev. Lett. **110**, 117206 (2013).

[57] V. Srinivasan, B. Godwal, J. C. Grossman, and R. Jeanloz, arXiv:1511.01989.

[58] D. L. Novikov, M. I. Katsnelson, A. V. Trefilov, A. J. Freeman, N. E. Christensen, A. Svane, and C. O. Rodriguez, Phys. Rev. B **59**, 4557 (1999).

[59] L. Dubrovinsky, N. Dubrovinskaia, E. Bykova, M. Bykov, V. Prakapenka, C. Prescher, K. Glazyrin, H.-P. Liermann, M. Hanfland, M. Ekholm, Q. Feng, L. V. Pourovskii, M. I. Katsnelson, J. M. Wills, and I. A. Abrikosov, Nature **525**, 226 (2015).